DOI 10.1007/s11182-019-01628-9

Russian Physics Journal, Vol. 61, No. 11, March, 2019 (Russian Original No. 11, November, 2018)

STRUCTURAL AND PHASE TRANSFROMATIONS IN SUPER-LOCALIZATION BAND IN Ni_3Ge SINGLE CRYSTAL

Yu. V. Solov'eva,[1] S. V. Starenchenko,[1] A. I. Ancharov,[2,3] and V. A. Starenchenko[1]

UDC 539.376:666.24/52-624

The paper studies the high-temperature plastic deformation in Ni_3Ge *alloy single crystals localizing in a band a few tens of microns wide that reaches the shear strain of thousands of percent. The electron backscatter diffraction and synchrotron radiation techniques allow investigating the structure of the single crystal in the band of super-localized plastic deformation. It is shown that super-localization of plastic deformation occurs due to the formation of polycrystalline multi-level substructure in the initial single crystal. The grain size and grain misorientation bimodal distributions are determined in the polycrystalline substructure. Also, regions of amorphous state are observed in the super-localization band at high homologous temperature* $T > 0.5T_m$. *A partial destruction of the far atomic order is detected.*

Keywords: $L1_2$ structure, intermetallic, super-localization, electron backscatter diffraction, synchrotron radiation.

INTRODUCTION

An intermetallic is a type of alloys having an ordered atomic arrangement in the crystal lattice sites that remains even up to the melting temperature. Intermetallic compounds are important components of many refractory superalloys [1]. High refractoriness of superalloys is conditioned by one of the most striking properties of intermetallic compounds, such as the anomalous (positive) temperature dependence of the yield and the flow stresses. This property is well-defined in intermetallic compounds with $L1_2$ structure among which there are binary nickel alloys, namely Ni_3Al, Ni_3Ga, Ni_3Si and others. Many publications are devoted to the nature of the temperature anomaly of mechanical properties intermetallic compounds [2]. Currently, research is being focused on the dislocation structures and the formation of dislocation barriers in superstrctures that play an important part in the process of the anomalous increase in stresses with the temperature growth [3–5]. Nevertheless, the problem of loss or decrease in the high-temperature properties of intermetallic compounds is still to be addressed. Traditionally, it is considered that in $L1_2$ alloys the flow stress decrease at temperatures exceeding the anomalous peak, involves the cubic crystal slip in the deformation process which replaces the octahedral crystal slip [6, 7]. However, at plastic deformation of [001]-oriented single crystals, the decrease in high-temperature flow stresses is not caused by the cubic crystal slip (the cubic slip system is not loaded). As is known, it is [001]-oriented single crystals that manifest the loss of stability during the high-temperature homogenous plastic deformation, when the flow stress curves non-monotonely decrease [8]. The high-temperature instability in the flow stress of intermetallic single crystals is determined by well-defined heterogeneity or macro- or

[1]Tomsk State University of Architecture and Building, Tomsk, Russia, e-mail: j_sol@mail.ru; sve-starenchenko@yandex.ru; star@tsuab.ru; [2]The Institute of Solid State Chemistry and Mechanochemistry of the Siberian Branch of the Russian Academy of Sciences, Novosibirsk, Russia, e-mail: ancharov@mail.ru; [3]Budker Institute of Nuclear Physics of the Siberian Branch of the Russian Academy of Sciences, Novosibirsk, Russia. Translated from Izvestiya Vysshikh Uchebnykh Zavedenii, Fizika, No. 11, pp. 35–41, November, 2018. Original article submitted August 15, 2018.

super-localized plastic deformation [9, 10]. Inside the non-deformable matrix, the crystals delaminate and form localized shear zones of intensive deformation. In super-localization bands this shear deformation achieves thousands of percent at the average total deformation of about 10 %. Our previous research into single crystals of Ni_3Ge alloy and widely used isostructural Ni_3Al alloy demonstrate that the local loss of stability of the dislocation structure occurs in the localized shear zone 50–80 μm thick. According to the scanning electron microscopy (SEM) observations, substructural transformations occur inside the super-localization band resulting in the formation of the band structure and the polycrystalline structure of dislocation [9]. However, several questions of the structural and phase transformations in the super-localization band remain open. On the one hand, it is necessary to study various properties of the polycrystalline structure inside the super-localization band, such as the grain size distribution, grain misorientation distribution, average grain size, *etc*. On the other hand, the phase composition should be identified, whether the far atomic order changes or not as well as the phase composition inside the super-localization band. The main purpose of this paper is to study the structure and phase composition of Ni3Ge alloy using the electron backscatter diffraction (EBSD) and synchrotron radiation techniques.

MATERIALS AND METHODS

The Bridgman method was used to grow single crystals of Ni_3Ge alloy in helium, in magnesium oxide crucibles. The homogeneous Ni_3Ge phase (β-phase) formed after the peritectic reaction at $T = 1405$ K had $L1_2$ structure with germanium (Ge) content ranged between 22.5 and 25 at.%. The crystal lattice parameter is $a = 3.57$ Å at Ge content of 25 at.% [11]. The single crystals were cut off the ingot using an electrospark discharge machine. The damaged layer was removed with abrasing machining, chemical etching in chlorazotic acid (HNO_3/HCl ratio 1:3), electropolishing in 80 g of Cr_2O_3 and 210 ml of H_3PO_4 electrolyte at 22 V during 2–3 min. The size of the initial samples was 2.5×2.5×5.0 mm. Homogenization of the samples was carried out in inert gas atmosphere at 953°C for 30 h followed by the sample cooling in a furnace down to room temperature. The crystal orientation was determined by the Laue method and the X-ray diffraction (XRD) analysis. The uniaxial compression tests were carried out on a test machine at 973 K, 3.5 10^{-2} s^{-1} strain rate and 10^{-2} Pa vacuum pressure.

EBSD investigations were performed on a dual-beam scanning electron microscope Quanta 200 3D (Netherlands) which uses the thermionic emission gun. The Quanta 200 3D was equipped with the Pegasus system, which combines energy dispersive spectroscopy and EBSD hardware. SEM observations were carried out at 30 kV accelerating voltage, 15 mm working distance and 2000× magnification. The scan areas were 136×790 and 13×33 μm with respectively 4 and 0.4 μm scan steps. Kikuchi lines formed by backscattered electrons were indexed automatically by the orientation imaging microscopy (OIM), developed by TexSEM Laboratories Inc. The measurement accuracy of orientation angles was 1°. The obtained data array was analyzed using the OIM analysis software.

The XRD analysis was conducted for the synchrotron radiation beam of the VEPP-3 storage ring, in Siberian Synchrotron and Terahertz Radiation Centre of the Budker Institute of Nuclear Physics SB RAS, Novosibirsk, Russia [12, 13]. Two-dimensional diffraction patterns were obtained for the X-ray beam propagation through the section area of the single crystal. Monochromatic synchrotron X-ray beam at a quantum energy of 33.7 keV and wavelength of 0.3685 Å was generated by the output collimating lens (beam size 0.1×0.4 mm) and passed across the sample. A MAR-345 detector was used for recording two-dimensional diffraction patterns. Specifications for the MAR-345 included a 345 mm detection area diameter, 100×100 μm spatial resolution, 2 min readout time, 72–426 mm sample-to-detector distance, and 0–65000 dynamic range.

RESULTS AND DISCUSSION

The structure and phase composition in the super-localization band were investigated under the following conditions. A 2.5×2.5×5.0 mm sample of Ni_3Ge single crystal with its end oriented parallel to (001) crystallographic plane, was subjected to the uniaxial compression at 973 K ($0.7T_m$) and $3.5 \cdot 10^{-2}$ s^{-1} strain rate. The axis direction of deformation was similar to the crystallographic direction [001]. In this experiment, the strain rate was one order

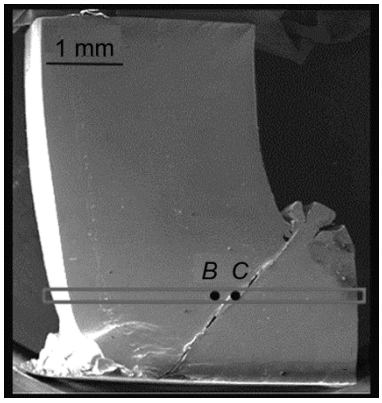

Fig. 1. Super-localized plastic deformation band on Ni_3Ge sample surface with [001] crystallographic direction. $\dot{\varepsilon} = 3.5 \cdot 10^{-2}\,\mathrm{s}^{-1}$, $T = 973$ K, $\varepsilon \approx 20.4\%$. Points *B* and *C* indicate places of examined microstructure.

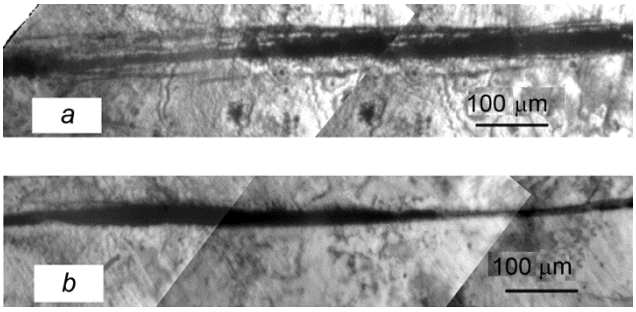

Fig. 2. Metallographic images of super-localization band depending of the strain rate: *a* – $\dot{\varepsilon} = 3.4 \cdot 10^{-3}\,\mathrm{s}^{-1}$, $l \approx 50\,\mu\mathrm{m}$; *b* – $\dot{\varepsilon} = 3.5 \cdot 10^{-2}\,\mathrm{s}^{-1}$, $l \approx 24\,\mu\mathrm{m}$. The microstructure is obtained by chemical etching after the removal of a 0.1 mm thick layer.

of magnitude greater than that in our early experiments [8]. As illustrated in Fig. 1, the single macro-localization band formed at the bottom of the sample. The shear strain in that band was about thousands of percent. When the shear in the upper part of the sample was restrained by the lower punch of the test machine, new macro-jogs appear on the opposite crystal edge with a single macro-jog. In Fig. 1, we indicated places in which the microstructure of the super-localization band was examined by the EBSD and synchrotron radiation techniques.

The metallographic study of the sample microstructure after the high-temperature deformation shows that the width of the super-localization band depends on the strain rate. Metallographic images of the obtained super-localization band are given in Fig. 2. When the strain rate is increased, the band width decreases twice and becomes well defined. This behavior indicates to the diffusion mechanisms describing the phenomenon of super-localized plastic deformation and the dependence of these mechanisms on the time period of activation of microscale processes.

EBSD investigations of the polished sample plane inside and within the super-localization band show that near the band the single crystal has a fragmented band structure. Misorientation bands are parallel to the super-localization band, and misorientation across the grain boundaries is not over 30 degrees (Fig. 3*a*). The dislocation band structure adjacent to the super-localization band is 300–350 μm wide.

As illustrated in Fig. 3*b*, the grain microstructure in the super-localization band is formed by equiaxial or rather elongated grains. The grain boundaries are typical for a dynamically recrystallized structure. Deformation-distorted grain boundaries and non-indexed areas are also observed nearby the grain boundaries indicated by black dots in

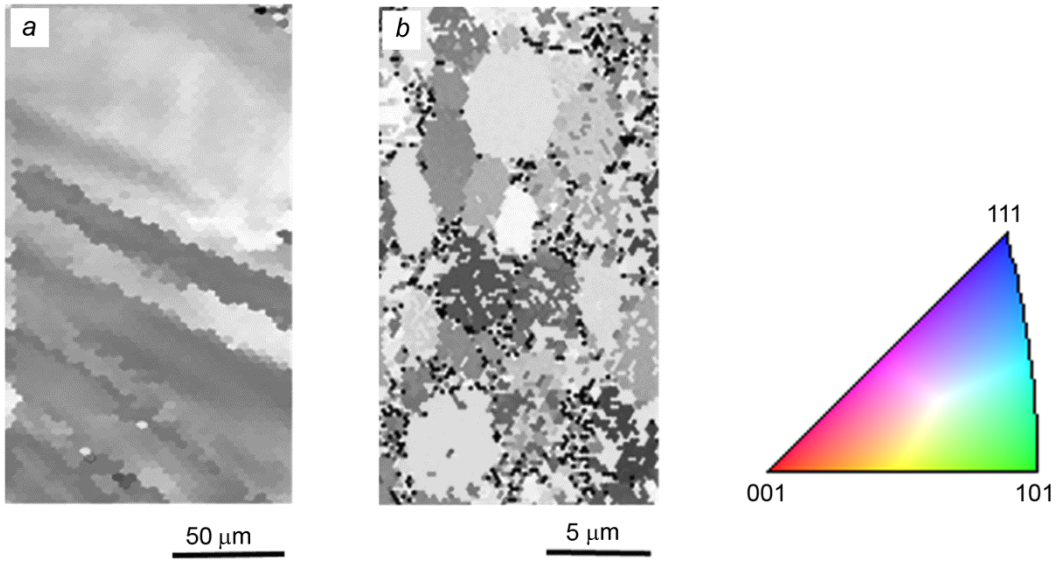

Fig. 3. EBSD maps of grain boundary misorientation distributions: *a* – near the super-localization band (*B* point in Fig. 1), *b* – inside the super-localization band (see Fig. 1, point *C*).

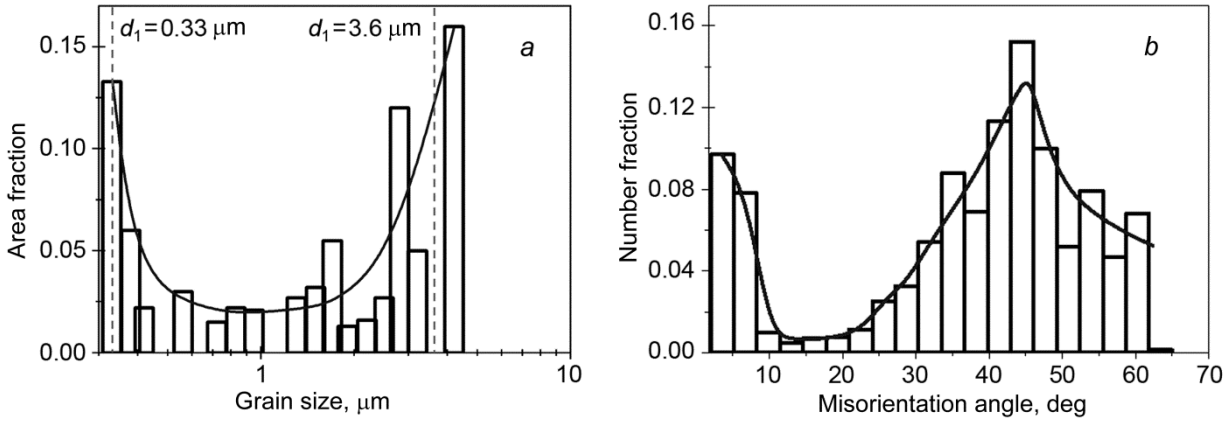

Fig. 4. Grain size distribution (*a*) and grain misorientation distribution (*b*) in super-localization band.

Fig. 3*b*. The grain structure formed inside the super-localization band is a multilevel structure. In Fig. 4*a*, two maximum values 0.33 and 3.6 μm are obtained for the area occupied by grains having different size. The analysis of EBSD map (Fig. 3*b*) shows that the coarse grains with the size of several micrometers have the inner structure, *i.e.* they are fragmented into submicron sized grains. In some cases, the crystal lattices of subgrains are misoriented relative to the main lattice of the grain. Also, there are traces of secondary recrystallization, such that subgrains fragment and occupy larger section area of the main grain. Such a structure indicates to the processes of the dynamic recovery, polygonization and recrystallization during the deformation localized in the narrow region of the single crystal. The dislocation glide and climb cause the grouping of dislocations into walls followed by the formation of the low-angle boundaries. The grain boundaries migrate toward the larger dislocation density with the addition of new dislocations. Due to this, the grain-boundary angles increase and form grains. A further development of this process leads to polygonization and recrystallization. The grains are divided into polygons, new grain nuclei appear, and secondary dynamic recrystallization occurs.

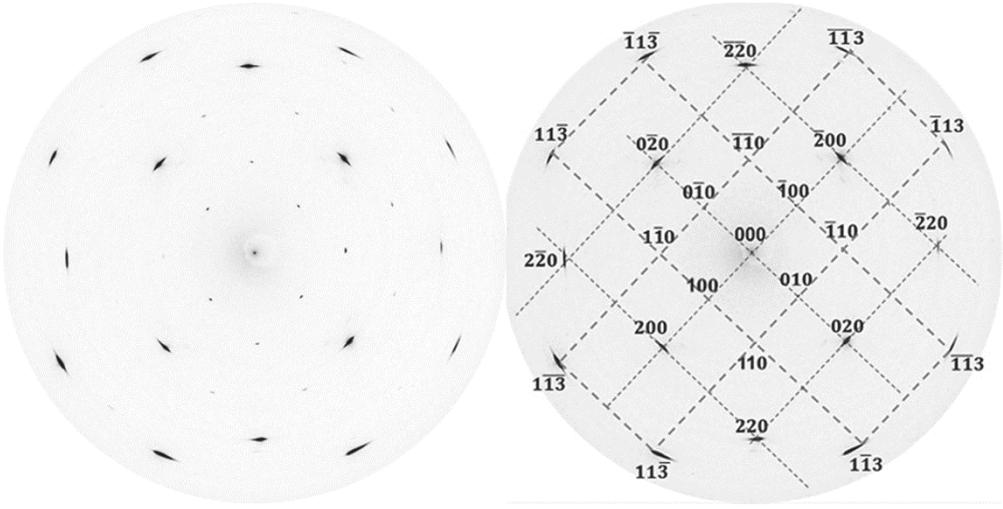

Fig. 5. Two-dimensional diffraction patterns of X-ray beam propagation through the section area of the crystal (see Fig. 1, point *B*). [001]-oriented Ni_3Ge single crystal after compressive deformation. $\dot{\varepsilon} = 3.5 \cdot 10^{-2}\ s^{-1}$, $T = 973$ K, $\varepsilon \approx 20.4\%$.

Using the dislocation kinetic model [14], we show that the dynamic processes can be cyclic. Under certain structural conditions, when new dislocations and point defects appear continuously during plastic deformation, cyclic scenarios of the defect structure development are possible, assuming the balance between the defect creation and elimination. The experimental study of the super-localization band shows that in reality, the structural changes are cyclic, that is characterized by the formation of low-angle boundaries and grains which increase in size and then divide into fragments, which, in turn also increase in size and fragment again. This dynamic process repeats many times. The structural analysis makes it possible to identify different stages of this dynamic process at different parts of the single crystal.

The diagram in Fig. 4*b* demonstrates the bimodal grain boundary distribution. There are two maximum values in this figure. The first relates to low-angle grain boundaries with a misorientation of 2–5 degrees or 10% of the total amount. The second relates to high-angle grain boundaries with a misorientation of 43–46 degrees or 15% of the total amount. Such a distribution reflects the process of the deformation-induced transition of the homogeneous dislocation structure to polycrystalline structure within the super-localization band. One can assume that the first maximum corresponds to subgrain boundaries forming as a result of polygonization into low-angle grain boundaries around subgrains. And the second maximum corresponds to high-angle grain boundaries forming as a result of the addition of new dislocations to low-angle grain boundaries during the dynamic recovery.

The XRD investigations and the synchrotron radiation are performed at the X-ray beam propagation through the sample region near and inside the super-localization band (see Fig. 1, points *B* and *C*). As shown in Fig. 5, the material near the super-localization band has a single-crystal structure. Diffraction patterns identify three reflecting crystallographic planes, namely (001) base plane and (031) and (301) planes whose grain-boundary angle is 18.4 degrees relative to (001) plane. It means that the radiation beam passes across three crystallites 0.1 mm in size. The inner structure of each crystallite is characterized by low-angle grain boundaries (azimuth misorientation 6–7°). The EBSD investigations prove that the structure near the super-localization band is single-crystal, with the grain-boundary angle not over 30 degrees.

The experiments demonstrate the fragmentation of the deformed single crystal in the super-localization band. A two-dimensional diffraction pattern from a circular aperture is presented in Fig. 6 for the synchrotron radiation beam propagating across the crystal inside the super-localization band. The general view of this XRD pattern indicates to its microcrystalline, misoriented structure. The rings are of a uniform contrast, without a high beam intensity that indicates to complete rupture of the single-crystal structure. Amorphous state is detected in the structure of the super-localization

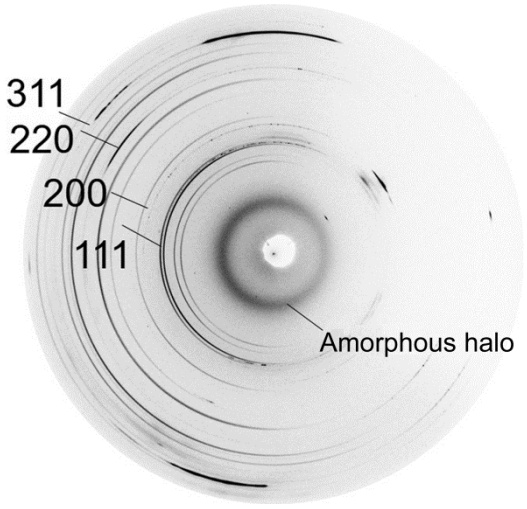

Fig. 6. Two-dimensional diffraction pattern from a circular aperture. Super-localization band structure obtained after plastic deformation (see Fig. 1, point *C*). [001]-oriented Ni_3Ge single crystal after compressive deformation. $\dot{\varepsilon} = 3.5 \cdot 10^{-2}\,\mathrm{s}^{-1}$, $T = 973$ K.

band as shown in Fig. 6. This fact is very interesting because amorphization of Ni_3Ge alloy *via* the conventional methods (Bridgeman anvil, equal channel angular extrusion, all-round compression, *etc*.) of plastic deformation is hard to achieve.

Another interesting fact is the amorphization process occurring at high homologous temperature ($T > 0.5T_m$). Supposedly, the amorphous phase forms at the grain boundaries appeared during the dynamic recrystallization. In EBSD maps presented in Fig. 3*b* they are indicated by black dots. The analysis of the XRD pattern (Fig. 6) shows that a strong non-equilibrium state in the super-localization band is based on $L1_2$ structure. There are lots of non-relaxing deformation defects which fragment the material and create the stress-strain state, thereby causing the lattice distortion. All this leads to the formation of the equilibrium, microcrystalline ordered structure, that is proved by the diffraction pattern describing the separation of the diffraction rings, may be due to the extensive defects of the packing and non-homogeneous stress state of the structure. The diffraction rings (110), (330) and (550) are detected in the structure and sectional diffraction rings (100), (300) and (500) – in the superstructure. If the greater part of the deformed material has the single-crystal structure with the far atomic order with $L1_2$ structure, the regular structure of the super-localization band ruptures due to the accumulation of the deformation defects and localized disordered regions.

CONCLUSIONS

This research allowed us to study the structural and phase transformations in the super-localization band of Ni_3Ge alloy single crystals. The obtained experimental results are in good agreement and mutually support each other.

1. Two regions appeared in the structure of the single crystal due to the formation of the super-localization band, *i.e*. the narrow, microcrystalline ordered structure 24–30 μm wide, the dislocation band structure nearby the super-localization band 300–350 μm wide, and the single crystalline zone with the low-angle band misorientation 300–350 μm wide nearby the super-localization band.

2. The grain structure in the narrow, microcrystalline region of the super-localization band had a multilevel structure.

3. Grain boundary and grain size bimodal distributions were obtained in the polycrystalline band. Two maximum values of 0.33 and 3.6 μm were detected in the area occupied by different grains. The first related to the low-

angle grain boundaries with misorientation of 2–5 degrees and the second – to the high-angle grain boundaries with misorientation of 43–46 degrees.

4. The regions of amorphous state were detected in the super-localization band.

5. Amorphization in the super-localization band occurred at high homologous temperatures ($T > 0.5T_m$).

6. A partial destruction of the long-range atomic order was detected in the super-localization band.

This work was financially supported by Grant N 16-03-00182-a from the Russian Foundation for Basic Research and carried out within the Project RFMEFI62117X0012 of the Ministry of Education and Science of the Russian Federation. The X-ray synchrotron measurements were conducted on VEPP-3/VEPP-4M storage ring and the Novosibirsk free electron laser (NovoFEL) radiation source in the Siberian Synchrotron and Terahertz Radiation Centre of the Budker Institute of Nuclear Physics SB RAS, Novosibirsk, Russia.

REFERENCES

1. Ch. T. Sims, N. S. Stoloff, and W. C. Hagel, Superalloys II [Russian translation], Metallurgiya, Moscow (1995), 384 p.
2. P. Veyssière and G. Saada, Dislocations in Solids, Chapter 53, F. R. N. Nabarro and M. S. Duesbery, eds., North-Holland Publishing Co., Elsevier Sci. Publ., Amsterdam (1996), p. 255.
3. W. Püschl, Mat. Sci. Eng. A, **319–321**, 266–269 (2001).
4. S. I. Rao, D. M. Dimiduk, T. A. Parthasarathy, *et al*., Scr. Mater., **66**, No. 6, 410–413 (2012).
5. A. Korner, H. P. Karnthaler, and C. Hitzenberger, Phil. Mag. A, **56**, No. 1, 73–88 (1987).
6. J. Michel, C. Coupeau, Y. Nahas, *et al*., Intermetallics, **50**, 86–93 (2014).
7. N. Frage, S. Kalabukhov, A. Wagner, and E. B. Zaretsky, Intermetallics, **102,** 26–33 (2018).
8. V. A. Starenchenko, E. V. Kozlov, Yu. V. Solov'eva, *et al*., Mat. Sci. Eng. A-Struct., **483–484**, No. 1–2, 602–606 (2008).
9. V. A. Starenchenko, Yu. V. Solov'eva, Ya. D. Fakhrutdinova, and L. A. Valuiskaya, Russ. Phys. J., **55**, No. 1, 62–73 (2012).
10. Yu. V. Solovieva, V. A. Starenchenko, B. I. Burtsev, *et al*., Bulletin of the Russian Academy of Sciences: Physics, **70,** No. 11, 1929–1931 (2006).
11. N. P. Lyakishev, ed., Phase Diagrams of Double Metal Systems: Reference Manual, in 3 vol., Mashinostroenie, Moscow (1997), 1024 p.
12. A. I. Ancharov, Russ. Phys. J., **60**, No. 3, 543–549 (2017).
13. P. A. Piminov, *et al*., Physics Procedia, **84**, 19–26 (2016).
14. V. A. Starenchenko, Yu. V. Solov'eva, Ya. D. Fakhrutdinova, and L. A. Valuiskaya, Russ. Phys. J., **54**, No. 8, 885–897 (2011).